Supplementary material for "Analyzing the effect of cell rearrangement on Delta-Notch pattern formation"

In this supplementary material, we provide the materials and methods for the experiments, the proof of the formulae and additional data for the numerical simulations and the experiments.

A. Materials and methods for experiments

Animals - H2B-mCherry transgenic mice were provided by the Laboratory for Animal Resources and Genetic Engineering, RIKEN Center for Developmental Biology [37]. All animals were handled in accordance with Nagoya University Guidelines on Laboratory Animal Welfare.

Cell mixing assay of mouse retinal vasculature - Neonatal mice at postnatal day 5 (P5) were anesthetized on crushed ice and sacrificed. Eyeballs were removed and placed in Hanks' Balanced Salt Solution in a 35-mm Petri dish. Using fine forceps, the periorbital connective tissue was removed from the eyeball. We made a small hole in the cornea using a 26G injection needle. Starting at the hole in the cornea, the sclera, choroid, and retinal pigment epithelia were peeled away. The retina was isolated from its anterior segment using microscissors [38] and cut into small pieces to prevent focus drift caused by retinal plane curvature. The retina was embedded in collagen gel solution (500 µl) and 1/1000 IB4-Alexa on a 35-mm Petri dish and incubated for 30 min at room temperature to allow the collagen gel to solidify. The dish was incubated for 30 min at 37°C to further solidify the collagen gel. We added 2 ml of medium [DMEM/F-12 + 10% FBS + 1/5000 isolectin B4 (IB4)-Alexa488 + 500 ng/ml FGF2] to the dish and visualized the blood vessels.

We performed time-lapse observations using a BX61 W1 upright microscope (Olympus), CSU-X1 (Yokogawa) with iXon+ EMCCD (Andor)(× 20, 5 min/frame, 12 h).

For cell tracking, we manually tracked the centers of cell nuclei with Fiji [39], using the TrackMate plugin [40]. We quantified the relative migration speed of the cell nuclei by dividing the relative migration length by the observation time. We defined the migration vector from the coordinates of the cell nuclei at the beginning and end of the imaging. The relative migration length of a cell is the length of the relative migration vector, which is calculated by subtracting the migration vector of a cell nucleus by the migration vector of the center of gravity of each cell group.

Cell proliferation assay of mouse retinal vasculature - For the proliferation assay for the endothelial cells in P5 mouse retinal vasculature, 30 µg/g bodyweight of 5-ethynyl-2'-deoxyuridine (EdU; Thermo Fisher Scientific) was intraperitoneally injected 2 h before sacrifice. After fixation with 4% paraformaldehyde in phosphate-buffered saline, the whole-mount retinas were processed with a Click-iT EdU Alexa Fluor 488 Imaging Kit (Thermo Fisher Scientific), in accordance with the manufacturer's instructions. To distinguish the endothelial cells, we performed immunohistochemistry using rabbit anti-Ets-related gene-1 (ERG1) monoclonal antibody (Abcam Ab92513) and Cy3-conjugated donkey anti-rabbit IgG secondary antibody (Jackson ImmunoResearch).

Images were taken using an LSM700 confocal microscope (Zeiss) with ZEN software (Zeiss) ($\times$ 20).

We counted the number of ERG1(+) cells and EdU(+) cells in five fields of view, and performed statistical analysis (Student's t-test) for a fraction of EdU(+) cells in ERG1(+) cells.

B. Experimental assay of cell mixing and proliferation

An example of Delta-Notch pattern formation on a one-dimensional line is the expression pattern of Delta-like ligand 4 (Dll4) mRNA in endothelial cells of the developing vasculature. Delta-like ligand 4 (Dll4) is a Notch ligand that is expressed mainly in the blood vessels, specifies the tip cells of growing vessels, and promotes arterialization [8, 13, 14]. In parallel with this specification, cell mixing and proliferation of endothelial cells occur in the developing vasculature [23, 24, 32–34].

It is reported that, in the retinal arteries of mice, Dll4 positive and negative cells alternately align, though in veins the expression level is low and almost homogeneous (Fig. S12(A)). Our theoretical results suggest that high motility or high proliferation rate of cells can contribute to the homogeneous expression pattern. Consistent with this hypothesis, venous endothelial cells have been reported to have greater motility and higher proliferation rates than arterial cells in the developing vasculature of zebrafish [33, 34]. We examined whether a similar difference in the motility and proliferation rate is observed in retinal vasculature in mice.

We examined the motility of the endothelial cells in veins and arteries by using an *ex vivo* assay, corresponding to the cell mixing model (5). We enucleated the eyes from the P5

mouse and isolated the retina. We cultured the retinal explants and tracked the movement of endothelial cells in the developing retinal vasculature for 12 h (Fig. S12(B)). In veins, endothelial cells actively migrated and exchanged their relative positions, though in the arteries the motility of the endothelial cells was lower and they rarely exchanged positions (Figs. S12(C), S12(D)). Cell displacements at 12 h were quantified, and the relative velocity of endothelial cells, which was calculated by dividing displacement, relative to the center of gravity of each cell group, by the observation time, was found to be 1.20 µm/h in veins and 0.74 µm/h in arteries (Fig. S12(D)). These velocities are significantly different from each other (p-value = 0.048). Note that the velocities of the ganglion cells were much smaller than those of the endothelial cells (Fig. S12(D)), supporting the hypothesis that the motion of the endothelial cells is active and did not arise passively from the deformation of the surrounding tissues.

Next, we examined the proliferation rate of endothelial cells in veins and arteries by an *in vivo* assay, corresponding to the cell proliferation model (7). Proliferation was assessed by EdU incorporation in 2 h in the postnatal mouse retinal vasculature *in vivo* (Figs. S12(E) and S12(F)). We intraperitoneally injected EdU 2 h before sacrifice and detected EdU incorporating cells. Since EdU was selectively incorporated by cells in the S phase, we could use this to identify proliferating cells. The fraction of EdU positive cells among endothelial cells, distinguished by the expression of ERG1, was 21.9% in veins and 9.8% in arteries (Fig. S12(F)). These percentages of EdU positive cells are significantly different from each other (p-value = 0.0001).

C. Approximation of (21) by a deterministic nonlocal evolution equation

The time evolution of the power spectrum (21) can be approximated by a deterministic nonlocal evolution equation by assuming that the number of cells n is sufficiently large.

Here, the k-th component of $d\boldsymbol{P}$ in (21) is:

$$\begin{aligned}\{d\boldsymbol{P}\}_k &= 2\mathrm{Re}[\lambda_{k-1}]\,\{\boldsymbol{P}\}_k + \{W\boldsymbol{P}dL_t^{pn}\}_k \\ &= 2\mathrm{Re}[\lambda_{k-1}]P_{k-1} + \left[16\sin^2\frac{\pi(k-1)}{n}\left(\frac{1}{n}\sum_{l=1}^{n}P_{l-1}\sin^2\frac{\pi(l-1)}{n}\right) - 8\sin^2\frac{\pi(k-1)}{n}P_{k-1}\right]\frac{dL_t^{pn}}{n} \\ &= 2\lambda(\theta_{k,n})P(\theta_{k,n}) + \left[16\sin^2\frac{\theta_{k,n}}{2}\left(\frac{1}{n}\sum_{l=0}^{n-1}P(\varphi_{l,n})\sin^2\frac{\varphi_{l,n}}{2}\right) - 8\sin^2\frac{\theta_{k,n}}{2}P(\theta_{k,n})\right]\frac{dL_t^{pn}}{n}.\end{aligned} \tag{S1}$$

Here, we set $\theta_{k,n} = 2\pi(k-1)/n$ and $\varphi_{l,n} = 2\pi(l-1)/n$, and regard the power spectrum P_k as a function of $\theta_{k,n}$. As $n \to \infty$, $\theta_{k,n} \to \theta$ and θ is dense in $[0, 2\pi)$, so that $P(\theta, t)$ becomes a continuous function of $\theta \in [0, 2\pi)$ and $t \in [0, \infty)$. Also, the diagonal matrix $\mathrm{Re}[\Lambda]$ is regarded as a multiplication operator with multiplication factor $2\lambda(\theta)$ where

$$\lambda(\theta) = \mathrm{Re}\left[\frac{-(a+d) + \sqrt{(a+d)^2 - 4(ad + 2b\alpha\cos\theta)}}{2}\right]. \tag{S2}$$

Using the fact that the Poisson process L_t^{pn}/n converges to pt as $n \to \infty$, so that $dL_t^{pn}/n \sim pdt$, then, by assuming $n \to \infty$,

$$\theta_{k,n} \xrightarrow{n\to\infty} \theta \quad (\theta \in [0, 2\pi)) \tag{S3}$$

$$\varphi_{l,n} \xrightarrow{n\to\infty} \varphi \quad (\varphi \in [0, 2\pi)) \tag{S4}$$

$$\frac{1}{n}\sum_{m=0}^{n-1} P(\varphi_{l,n}) \sin^2\frac{\varphi_{l,n}}{2} \xrightarrow{n\to\infty} \frac{1}{2\pi}\int_0^{2\pi} P(\varphi)\sin^2\frac{\varphi}{2} d\varphi \tag{S5}$$

$$\frac{dL_t^{pn}}{n} \xrightarrow{n\to\infty} pdt. \tag{S6}$$

Therefore, (21) is approximated by a system of deterministic nonlocal evolution equations as:

$$\begin{aligned}\frac{d}{dt}P(\theta,t) &= \left(2\lambda(\theta) - 8p\sin^2\frac{\theta}{2}\right)P(\theta,t) \\ &\quad + \frac{8}{\pi}p\sin^2\frac{\theta}{2}\int_0^{2\pi} P(\varphi,t)\sin^2\frac{\varphi}{2}d\varphi \\ &= \mathcal{Y}_p(P(\theta,t)),\end{aligned} \tag{S7}$$

where $\mathcal{Y}_p$ is the operator acting on $P(\theta, t)$. Therefore, by using the maximum eigenvalue and the corresponding eigenfunction of the operator $\mathcal{Y}_p$, we can derive the expected pattern dynamics.

From the Perron-Frobenius theorem and its extension to the integral operator by Jentzsch [41], the eigenvalue y corresponding to the positive eigenfunction $P^*(\theta) > 0$ is the maximum eigenvalue of the operator $\mathcal{Y}_p$. By substituting the eigenvalue y and the corresponding eigenfunction $P^*(\theta)$ of the operator $\mathcal{Y}_p$ into (S7), we have:

$$P^*(\theta) = \frac{\frac{8}{\pi}p\sin^2\frac{\theta}{2}\int_0^{2\pi} P^*(\varphi)\sin^2\frac{\varphi}{2}d\varphi}{y + 8p\sin^2\frac{\theta}{2} - 2\lambda(\theta)}. \tag{S8}$$

Hence we obtain a recursive relation for $P^*(\theta)$:

$$\int_0^{2\pi} P^*(\theta)\sin^2\frac{\theta}{2}d\theta \\ = \frac{8}{\pi}\int_0^{2\pi}\frac{p\sin^4\frac{\theta}{2}\int_0^{2\pi}P^*(\varphi)\sin^2\frac{\varphi}{2}d\varphi}{y+8p\sin^2\frac{\theta}{2}-2\lambda(\theta)}d\theta. \tag{S9}$$

Assuming $P^*(\theta) > 0$ ($\forall\theta \in [0, 2\pi)$), the integral of $P^*(\theta)\sin^2(\theta/2)$ is a constant positive value, and we can obtain the eigenvalue y of the operator $\mathcal{Y}_p$ as the solution of the integral equation:

$$\pi = \int_0^{2\pi}\frac{8p\sin^4(\phi/2)}{y+8p\sin^2(\phi/2)-2\lambda(\phi)}d\phi, \tag{S10}$$

and the corresponding eigenfunction $P^*(\theta)$ is:

$$P^*(\theta) = \frac{8p\sin^2(\theta/2)}{y+8p\sin^2(\theta/2)-2\lambda(\theta)}. \tag{S11}$$

We can also obtain the balanced frequency p^* as the solution of the integral equation that is obtained by substituting $y = 0$ into (S10) as below:

$$\pi = \int_0^{2\pi}\frac{4p^*\sin^4(\phi/2)}{4p^*\sin^2(\phi/2)-\lambda(\phi)}d\phi. \tag{S12}$$

D. Proof of the trigonometric formulae in Appendix C

In this section, we prove the formulae that are used in Appendix C, namely

$$\sum_{l=0}^{n-1}\frac{1}{n(n+1)}\frac{\sin^2\frac{\pi l}{n}}{\sin^2\left(\frac{\pi k}{n+1}-\frac{\pi l}{n}\right)} = 1+\frac{2}{n+1}\cos\frac{2\pi k}{n+1}. \tag{S13}$$

$$\sum_{l=0}^{n-1}\frac{1}{n(n+1)}\frac{\sin^2\frac{\pi l}{n}}{\sin^2\left(\frac{\pi k}{n+1}-\frac{\pi l}{n}\right)}\cos\frac{2\pi ml}{n} = \frac{n-m+1}{n+1}\cos\frac{2\pi km}{n+1}+\frac{m+1}{n+1}\cos\frac{2\pi k(m+1)}{n+1}. \tag{S14}$$

Here, k, l, m and n are integers, and $n \geq 2$, $k \in [1, n-1]$ and $m \in [1, n-1]$.

For (S13), we start from the formulae for $x \neq (\pi l/n)$ (l is an arbitrary integer) that are obtained in [42, 43]:

$$\sum_{l=0}^{n-1}\frac{1}{\sin^2\left(x+\frac{\pi l}{n}\right)} = \frac{n^2}{\sin^2(nx)}, \tag{S15}$$

$$\sum_{l=0}^{n-1}\cot\left(x+\frac{\pi l}{n}\right) = n\cot(nx). \tag{S16}$$

By substituting $x = -\pi k/(n+1)$ into (S15) and (S16), we obtain:

$$\sum_{l=0}^{n-1} \frac{\sin^2 \frac{\pi k}{n+1}}{\sin^2\left(\frac{\pi l}{n} - \frac{\pi k}{n+1}\right)} = n^2, \tag{S17}$$

$$\sum_{l=0}^{n-1} \cot\left(\frac{\pi l}{n} - \frac{\pi k}{n+1}\right) = n \cot \frac{\pi k}{n+1}. \tag{S18}$$

Here we used the periodicity of $\sin^2 x$ and $\cot x$ (period length $= \pi$) such that:

$$\sin^2\left(-\frac{n\pi k}{n+1}\right) = \sin^2\left(-\pi k + \frac{\pi k}{n+1}\right) = \sin^2\left(\frac{\pi k}{n+1}\right), \tag{S19}$$

$$\cot\left(-\frac{n\pi k}{n+1}\right) = \cot\left(-\pi k + \frac{\pi k}{n+1}\right) = \cot\left(\frac{\pi k}{n+1}\right). \tag{S20}$$

We consider the finite summation as below:

$$\begin{aligned}
\sum_{l=0}^{n-1} \frac{\sin^2 \frac{\pi l}{n} - \sin^2 \frac{\pi k}{n+1}}{\sin^2\left(\frac{\pi l}{n} - \frac{\pi k}{n+1}\right)} &= \sum_{l=0}^{n-1} \frac{\sin\left(\frac{\pi l}{n} + \frac{\pi k}{n+1}\right)}{\sin\left(\frac{\pi l}{n} - \frac{\pi k}{n+1}\right)} \\
&= \sum_{l=0}^{n-1} \frac{\sin\left(\frac{\pi l}{n} - \frac{\pi k}{n+1} + \frac{2\pi k}{n+1}\right)}{\sin\left(\frac{\pi l}{n} - \frac{\pi k}{n+1}\right)} \\
&= n \cos \frac{2\pi k}{n+1} + \sin \frac{2\pi k}{n+1} \sum_{l=0}^{n-1} \cot\left(\frac{\pi l}{n} - \frac{\pi k}{n+1}\right) \\
&= n\left(\cos \frac{2\pi k}{n+1} + \sin \frac{2\pi k}{n+1} \cot \frac{\pi k}{n+1}\right) \\
&= n\left(1 + 2\cos \frac{2\pi k}{n+1}\right).
\end{aligned} \tag{S21}$$

Here we used the formula:

$$\sin^2 \alpha - \sin^2 \beta = \frac{1}{2}(\cos 2\beta - \cos 2\alpha) = \sin(\alpha+\beta)\sin(\alpha-\beta), \tag{S22}$$

and the trigonometric addition formulae. From (S17) and (S21), we obtain:

$$\sum_{l=0}^{n-1} \frac{\sin^2 \frac{\pi l}{n}}{\sin^2\left(\frac{\pi k}{n+1} - \frac{\pi l}{n}\right)} = n^2 + n + 2n \cos \frac{2\pi k}{n+1}. \tag{S23}$$

Therefore, we obtain (S13) by dividing both sides of (S23) by $n(n+1)$.

For (S14), we start from the formula:

$$\begin{aligned}
\sin^2 \frac{\pi l}{n} \cos \frac{2\pi m l}{n} &= \frac{1}{2}\left(1 - \cos \frac{2\pi l}{n}\right) \cos \frac{2\pi m l}{n} \\
&= -\frac{1}{4} \cos \frac{2\pi(m-1)l}{n} + \frac{1}{2} \cos \frac{2\pi m l}{n} - \frac{1}{4} \cos \frac{2\pi(m+1)l}{n}
\end{aligned}, \tag{S24}$$

and use it to transform the right-hand of (S14) as follows:

$$\frac{1}{n+1}\left(\frac{1}{2}\mathcal{D}_m - \frac{1}{4}\mathcal{D}_{m-1} - \frac{1}{4}\mathcal{D}_{m+1}\right), \tag{S25}$$

where

$$\mathcal{D}_m = \frac{1}{n}\sum_{l=0}^{n-1} \frac{\cos\frac{2\pi ml}{n}}{\sin^2(\frac{\pi k}{n+1} - \frac{\pi l}{n})}. \tag{S26}$$

We consider the finite summation as below:

$$\begin{aligned}
\mathcal{A}_m =& \frac{1}{n}\sum_{l=0}^{n-1} \frac{\cos\frac{2\pi mk}{n+1} - \cos\frac{2\pi ml}{n}}{\sin^2(\frac{\pi k}{n+1} - \frac{\pi l}{n})} \\
=& \, 2\cos\frac{2\pi mk}{n+1}\left(\frac{1}{n}\sum_{l=0}^{n-1} \frac{\sin^2 m(\frac{\pi k}{n+1} - \frac{\pi l}{n})}{\sin^2(\frac{\pi k}{n+1} - \frac{\pi l}{n})}\right) - 2\sin\frac{2\pi mk}{n+1}\left(\frac{1}{n}\sum_{l=0}^{n-1} \frac{\sin m(\frac{\pi k}{n+1} - \frac{\pi l}{n})\cos m(\frac{\pi k}{n+1} - \frac{\pi l}{n})}{\sin^2(\frac{\pi k}{n+1} - \frac{\pi l}{n})}\right) \\
=& \, 2\cos\frac{2\pi mk}{n+1}\mathcal{B}_m - 2\sin\frac{2\pi mk}{n+1}\mathcal{C}_m.
\end{aligned} \tag{S27}$$

Here we used the formula:

$$\begin{aligned}
\cos\frac{2\pi mk}{n+1} - \cos\frac{2\pi ml}{n} =& -2\sin m\left(\frac{\pi k}{n+1} + \frac{\pi l}{n}\right)\sin m\left(\frac{\pi k}{n+1} - \frac{\pi l}{n}\right) \\
=& \, 2\left(\sin^2 m\left(\frac{\pi k}{n+1} - \frac{\pi l}{n}\right)\cos\frac{2\pi mk}{n+1}\right. \\
& \left. - \cos m\left(\frac{\pi k}{n+1} - \frac{\pi l}{n}\right)\sin m\left(\frac{\pi k}{n+1} - \frac{\pi l}{n}\right)\sin\frac{2\pi mk}{n+1}\right),
\end{aligned} \tag{S28}$$

and define

$$\mathcal{B}_m = \frac{1}{n}\sum_{l=0}^{n-1} \frac{\sin^2 m(\frac{\pi k}{n+1} - \frac{\pi l}{n})}{\sin^2(\frac{\pi k}{n+1} - \frac{\pi l}{n})}, \tag{S29}$$

$$\mathcal{C}_m = \frac{1}{n}\sum_{l=0}^{n-1} \frac{\sin m(\frac{\pi k}{n+1} - \frac{\pi l}{n})\cos m(\frac{\pi k}{n+1} - \frac{\pi l}{n})}{\sin^2(\frac{\pi k}{n+1} - \frac{\pi l}{n})}. \tag{S30}$$

For (S29), we define $\Delta\mathcal{B}_m$ as the difference between $\mathcal{B}_{m+1}$ and $\mathcal{B}_m$:

$$\begin{aligned}
\Delta\mathcal{B}_m =& \, \mathcal{B}_{m+1} - \mathcal{B}_m \\
=& \frac{1}{2n}\sum_{l=0}^{n-1} \frac{\cos\left[2m(\frac{\pi k}{n+1} - \frac{\pi l}{n})\right] - \cos\left[2(m+1)(\frac{\pi k}{n+1} - \frac{\pi l}{n})\right]}{\sin^2(\frac{\pi k}{n+1} - \frac{\pi l}{n})} \\
=& \frac{1}{2n}\sum_{l=0}^{n-1} \frac{2\sin\left[(2m+1)(\frac{\pi k}{n+1} - \frac{\pi l}{n})\right]\sin(\frac{\pi k}{n+1} - \frac{\pi l}{n})}{\sin^2(\frac{\pi k}{n+1} - \frac{\pi l}{n})} \\
=& \frac{1}{n}\sum_{l=0}^{n-1} \frac{\sin\left[(2m+1)(\frac{\pi k}{n+1} - \frac{\pi l}{n})\right]}{\sin(\frac{\pi k}{n+1} - \frac{\pi l}{n})}.
\end{aligned} \tag{S31}$$

Here we used the formula:

$$\sin^2\left[m\left(\frac{\pi k}{n+1}-\frac{\pi l}{n}\right)\right]=\frac{1-\cos\left[2m(\frac{\pi k}{n+1}-\frac{\pi l}{n})\right]}{2}. \tag{S32}$$

We also obtain the difference between $\Delta\mathcal{B}_{m+1}$ and $\Delta\mathcal{B}_m$:

$$\begin{aligned}\Delta\mathcal{B}_{m+1}-\Delta\mathcal{B}_m&=\frac{1}{n}\sum_{l=0}^{n-1}\frac{\sin\left[(2m+3)(\frac{\pi k}{n+1}-\frac{\pi l}{n})\right]-\sin\left[(2m+1)(\frac{\pi k}{n+1}-\frac{\pi l}{n})\right]}{\sin(\frac{\pi k}{n+1}-\frac{\pi l}{n})}\\&=\frac{1}{n}\sum_{l=0}^{n-1}\frac{2\cos\left[2(m+1)(\frac{\pi k}{n+1}-\frac{\pi l}{n})\right]\sin(\frac{\pi k}{n+1}-\frac{\pi l}{n})}{\sin(\frac{\pi k}{n+1}-\frac{\pi l}{n})}\\&=\frac{1}{n}\sum_{l=0}^{n-1}2\cos\left[2(m+1)\left(\frac{\pi k}{n+1}-\frac{\pi l}{n}\right)\right]\\&=0.\end{aligned} \tag{S33}$$

The relationship (S33) holds for any $m\in\mathbb{N}$. This means that $\Delta\mathcal{B}_m$ takes the same value independent of m:

$$\Delta\mathcal{B}_m=\Delta\mathcal{B}_0=\frac{1}{n}\sum_{\kappa=0}^{n-1}1=1. \tag{S34}$$

Since $\mathcal{B}_1=1$, we obtain:

$$\mathcal{B}_m=\mathcal{B}_1+\sum_{\kappa=1}^{m-1}1=m. \tag{S35}$$

For (S30), we define $\Delta\mathcal{C}_m$ as the difference between $\mathcal{C}_{m+1}$ and $\mathcal{C}_m$:

$$\begin{aligned}\Delta\mathcal{C}_m&=\mathcal{C}_{m+1}-\mathcal{C}_m\\&=\frac{1}{2n}\sum_{l=0}^{n-1}\frac{\sin\left[2m(\frac{\pi k}{n+1}-\frac{\pi l}{n})\right]-\sin\left[2(m+1)(\frac{\pi k}{n+1}-\frac{\pi l}{n})\right]}{\sin^2(\frac{\pi k}{n+1}-\frac{\pi l}{n})}\\&=\frac{1}{2n}\sum_{l=0}^{n-1}\frac{2\cos\left[(2m+1)(\frac{\pi k}{n+1}-\frac{\pi l}{n})\right]\sin(\frac{\pi k}{n+1}-\frac{\pi l}{n})}{\sin^2(\frac{\pi k}{n+1}-\frac{\pi l}{n})}\\&=\frac{1}{n}\sum_{l=0}^{n-1}\frac{\cos\left[(2m+1)(\frac{\pi k}{n+1}-\frac{\pi l}{n})\right]}{\sin(\frac{\pi k}{n+1}-\frac{\pi l}{n})}.\end{aligned} \tag{S36}$$

Here we used the formula:

$$\sin\left[m\left(\frac{\pi k}{n+1}-\frac{\pi l}{n}\right)\right]\cos\left[m\left(\frac{\pi k}{n+1}-\frac{\pi l}{n}\right)\right]=\frac{1}{2}\sin\left[2m\left(\frac{\pi k}{n+1}-\frac{\pi l}{n}\right)\right]. \tag{S37}$$

We also obtain the difference between $\Delta\mathcal{C}_{m+1}$ and $\Delta\mathcal{C}_m$:

$$\begin{aligned}\Delta\mathcal{C}_{m+1} - \Delta\mathcal{C}_m &= \frac{1}{n}\sum_{l=0}^{n-1} \frac{\cos\left[(2m+3)(\frac{\pi k}{n+1} - \frac{\pi l}{n})\right] - \cos\left[(2m+1)(\frac{\pi k}{n+1} - \frac{\pi l}{n})\right]}{\sin(\frac{\pi k}{n+1} - \frac{\pi l}{n})} \\ &= \frac{1}{n}\sum_{l=0}^{n-1} \frac{-2\sin\left[2(m+1)(\frac{\pi k}{n+1} - \frac{\pi l}{n})\right]\sin(\frac{\pi k}{n+1} - \frac{\pi l}{n})}{\sin(\frac{\pi k}{n+1} - \frac{\pi l}{n})} \\ &= \frac{1}{n}\sum_{l=0}^{n-1} -2\sin\left[2(m+1)\left(\frac{\pi k}{n+1} - \frac{\pi l}{n}\right)\right] \\ &= 0. \end{aligned} \tag{S38}$$

The relationship (S38) holds for any $m \in \mathbb{N}$. Hence $\Delta\mathcal{C}_m$ takes the same value independent of m:

$$\Delta\mathcal{C}_m = \Delta\mathcal{C}_0 = \frac{1}{n}\sum_{l=0}^{n-1} \frac{\cos(\frac{\pi k}{n+1} - \frac{\pi l}{n})}{\sin(\frac{\pi k}{n+1} - \frac{\pi l}{n})} = \cot\frac{\pi k}{n+1}. \tag{S39}$$

Here we used equation (S18). Since $\mathcal{C}_1 = \cot(\pi k/(n+1))$, we obtain:

$$\mathcal{C}_m = m\cot\frac{\pi k}{n+1}. \tag{S40}$$

By substituting (S35) and (S40) into (S27), we obtain:

$$\begin{aligned}\mathcal{A}_m &= 2m\cos\frac{2\pi mk}{n+1} - 2m\cot\frac{\pi k}{n+1}\sin\frac{2\pi mk}{n+1} \\ &= -2m\frac{\sin\frac{(2m+1)\pi k}{n+1}}{\sin\frac{\pi k}{n+1}} \\ &= -2m - 4m\left(\cos\frac{2\pi k}{n+1} + \cos\frac{4\pi k}{n+1} + \cdots + \cos\frac{2\pi mk}{n+1}\right). \end{aligned} \tag{S41}$$

Here we used the relationship:

$$\left(\sum_{\kappa=1}^{m}\cos\frac{2\kappa\pi k}{n+1}\right)\sin\frac{\pi k}{n+1} = \frac{1}{2}\left(\sin\frac{(2m+1)\pi k}{n+1} - \sin\frac{\pi k}{n+1}\right), \tag{S42}$$

which is derived from the formula:

$$\cos\frac{2\pi mk}{n+1}\sin\frac{\pi k}{n+1} = \frac{1}{2}\left(\sin\frac{(2m+1)\pi k}{n+1} - \sin\frac{(2m-1)\pi k}{n+1}\right). \tag{S43}$$

From (S41) and (S17), we obtain:

$$\mathcal{D}_m = \frac{n}{\sin^2\frac{\pi k}{n+1}}\cos\frac{2\pi mk}{n+1} - \left(2m + 4m\left(\cos\frac{2\pi k}{n+1} + \cos\frac{4\pi k}{n+1} + \cdots + \cos\frac{2\pi mk}{n+1}\right)\right). \tag{S44}$$

767 Therefore, we have:

$$\begin{aligned}\frac{1}{2}D_m - \frac{1}{4}D_{m-1} - \frac{1}{4}D_{m+1} =& -(m-1)\cos\frac{2\pi mk}{n+1} + (m+1)\cos\frac{2(m+1)\pi k}{n+1} \\ &+ \frac{n}{\sin^2\frac{\pi k}{n+1}}\sin^2\frac{\pi k}{n+1}\cos\frac{2\pi mk}{n+1} \\ =&(n-m+1)\cos\frac{2\pi mk}{n+1} + (m+1)\cos\frac{2(m+1)\pi k}{n+1}. \end{aligned} \tag{S45}$$

768 Here we used the formula:

$$2\cos\frac{2m\pi k}{n+1} - \cos\frac{2(m-1)\pi k}{n+1} - \cos\frac{2(m+1)\pi k}{n+1} = 4\sin^2\frac{\pi k}{n+1}\cos\frac{2m\pi k}{n+1}. \tag{S46}$$

769 Therefore, we obtain (S14) by dividing both sides of (S45) by $(n+1)$.

E. Analysis of the cis-inhibition model with cell rearrangement

Sprinzak *et al.* [3] proposed the following model that includes cis-inhibition, which is the inhibition of Notch activity by the Delta activity in a single cell:

$$\begin{aligned}
\frac{d}{dt}N_x &= \beta_N - N_x - N_x \langle D_j \rangle_x - N_x \frac{D_x}{k_c} \\
\frac{d}{dt}D_x &= \beta_D \frac{1}{1+R_x^m} - D_x - \langle N_j \rangle_x D_x - N_x \frac{D_x}{k_c} \\
\frac{d}{dt}R_x &= \beta_R \frac{\left(N_x \langle D_j \rangle_x\right)^p}{k_{rs}^p + \left(N_x \langle D_j \rangle_x\right)^p} - R_x.
\end{aligned} \tag{S47}$$

Here, N_x, D_x and R_x are, respectively, the Notch, Delta and a Reporter of Notch signaling activities of the cell x, and $\langle D_j \rangle_x = (D_{x-1} + D_{x+1})/2$ and $\langle N_j \rangle_x = (N_{x-1} + N_{x+1})/2$. This reporter represents the transcriptional activity resulting from Delta-Notch binding. We performed numerical simulations and analysis of the model (S47) in a one-dimensional cell array with periodic boundary conditions. We set $p = 1$ to match the numerical simulations in the original article [3].

For the linear stability analysis, the homogeneous steady state (N^0, D^0, R^0) in the model (S47) satisfies the equations:

$$\begin{aligned}
&\beta_N - N^0 - N^0 D^0 - N^0 \frac{D^0}{k_c} = 0 \\
&\beta_D \frac{1}{1+(R^0)^m} - D^0 - N^0 D^0 - N^0 \frac{D^0}{k_c} = 0 \\
&\beta_R \frac{(N^0 D^0)}{k_{rs} + (N^0 D^0)} - R^0 = 0.
\end{aligned} \tag{S48}$$

By assuming $(N_x, D_x, R_x) = (N^0 + n_x, D^0 + d_x, R^0 + r_x)$, $|n_x| \ll N^0$, $|d_x| \ll D^0$ and $|r_x| \ll R^0$, we can linearize the model (S47):

$$\frac{d}{dt}\boldsymbol{u}_{\boldsymbol{x}}(t) = M\boldsymbol{u}_x(t) + L\bar{\boldsymbol{u}}_x(t). \tag{S49}$$

Here, $\boldsymbol{u}_x(t) = (n_x(t), d_x(t), r_x(t))^{\mathsf{T}}$, $\bar{\boldsymbol{u}}_x(t) = (\boldsymbol{u}_{x-1} + \boldsymbol{u}_{x+1})/2$,

$$M = \begin{pmatrix} -\frac{D^0}{k_c} - D^0 - 1 & -\frac{N^0}{k_c} & 0 \\ -\frac{D^0}{k_c} & -\frac{N^0}{k_c} - N^0 - 1 & -\frac{m(R^0)^{m-1}\beta_D}{\left((R^0)^m+1\right)^2} \\ \frac{\beta_R D^0 k_{rs}}{(D^0 N^0 + k_{rs})^2} & 0 & -1 \end{pmatrix} \tag{S50}$$

and

$$L = \begin{pmatrix} 0 & -N^0 & 0 \\ -D^0 & 0 & 0 \\ 0 & \frac{k_{rs}N^0\beta_R}{(k_{rs}+D^0N^0)^2} & 0 \end{pmatrix}. \tag{S51}$$

Then, we obtain:

$$\frac{d}{dt}\hat{\boldsymbol{u}}_k(t) = \left(M + L\cos\frac{2\pi k}{n}\right)\hat{\boldsymbol{u}}_k(t). \tag{S52}$$

Here, $\hat{\boldsymbol{u}}_k(t)$ is the discrete Fourier transformation of $\boldsymbol{u}_x(t)$. The dispersion relation $\lambda(k)$ is derived as the largest eigenvalue of the matrix $(M + L\cos k)$ (Fig. S14(A)).

Supplementary Figure 14(B) shows that the Sprinzak model [3] also generates the salt and pepper pattern as long as the maximum value of $\lambda(k)$ is positive, showing that the linear stability analysis determines the conditions for pattern formation.

For the Sprinzak model with cell mixing and proliferation, we can calculate the balanced frequencies p^* and q^* by solving the eigenvalue problem as in (23) and (39). Figure S14(C) shows that the values of p^* and q^* are in good agreement with the numerically estimated values. These results show that our analysis can be applied to other pattern formation mechanisms.

Parameters	H_0
$r = 40, \beta = 100$	$2.03 * 10^{-10}$
$r = 40, \beta = 120$	$5.74 * 10^{-11}$
$r = 40, \beta = 140$	$6.46 * 10^{-11}$
$r = 40, \beta = 160$	$5.60 * 10^{-11}$
$r = 40, \beta = 180$	$5.29 * 10^{-11}$
$r = 40, \beta = 200$	$6.85 * 10^{-11}$
$r = 25, \beta = 100$	$1.88 * 10^{-10}$
$r = 30, \beta = 100$	$1.35 * 10^{-10}$
$r = 35, \beta = 100$	$7.74 * 10^{-11}$

Supplementary Table 1. H_0 values used to calculate H^*. H_0 values are calculated from the numerical simulation of the Collier model (1), shown in Fig. S4.

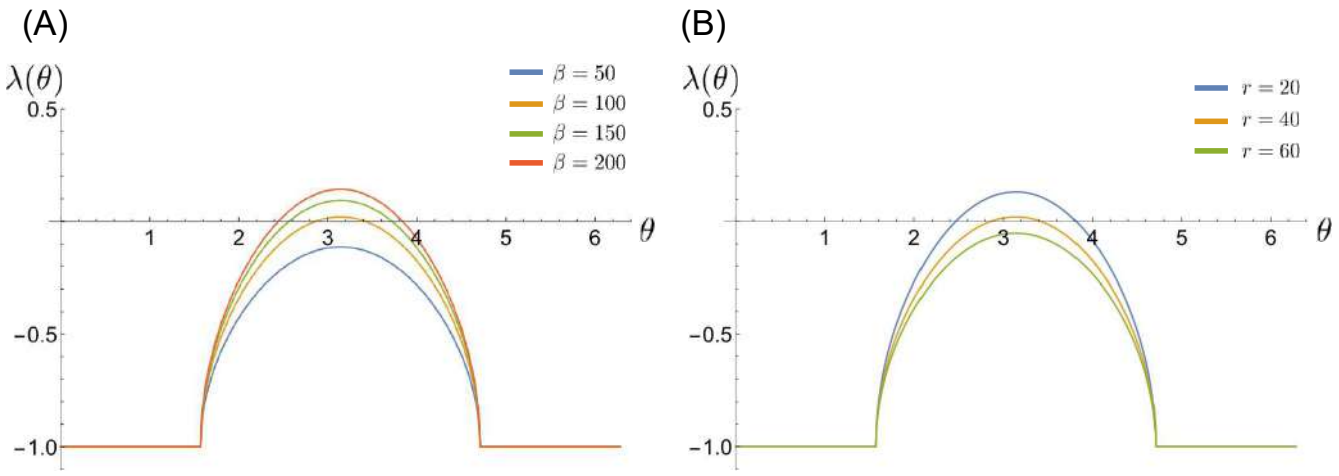

Supplementary Figure 1. Plots of the dispersion-relation for the version of the Collier model we use (1). $\lambda(\theta)$ is the real part of the larger eigenvalue in (A9) and $\theta = 2\pi k/n$. (A) The dispersion-relation for several values of β. $\lambda(\theta)$ is negative for any k when $\beta = 50$ and takes positive values in a narrow region around $\theta = \pi$ when $\beta = 100$. As β increases, the region where $\lambda(\theta)$ takes positive values broadens. (B) The dispersion-relation for several values of r. A similar relationship as for β is obtained, but the region where $\lambda(\theta)$ takes positive values becomes narrower as r increases. The other parameters are as in Fig. 2.

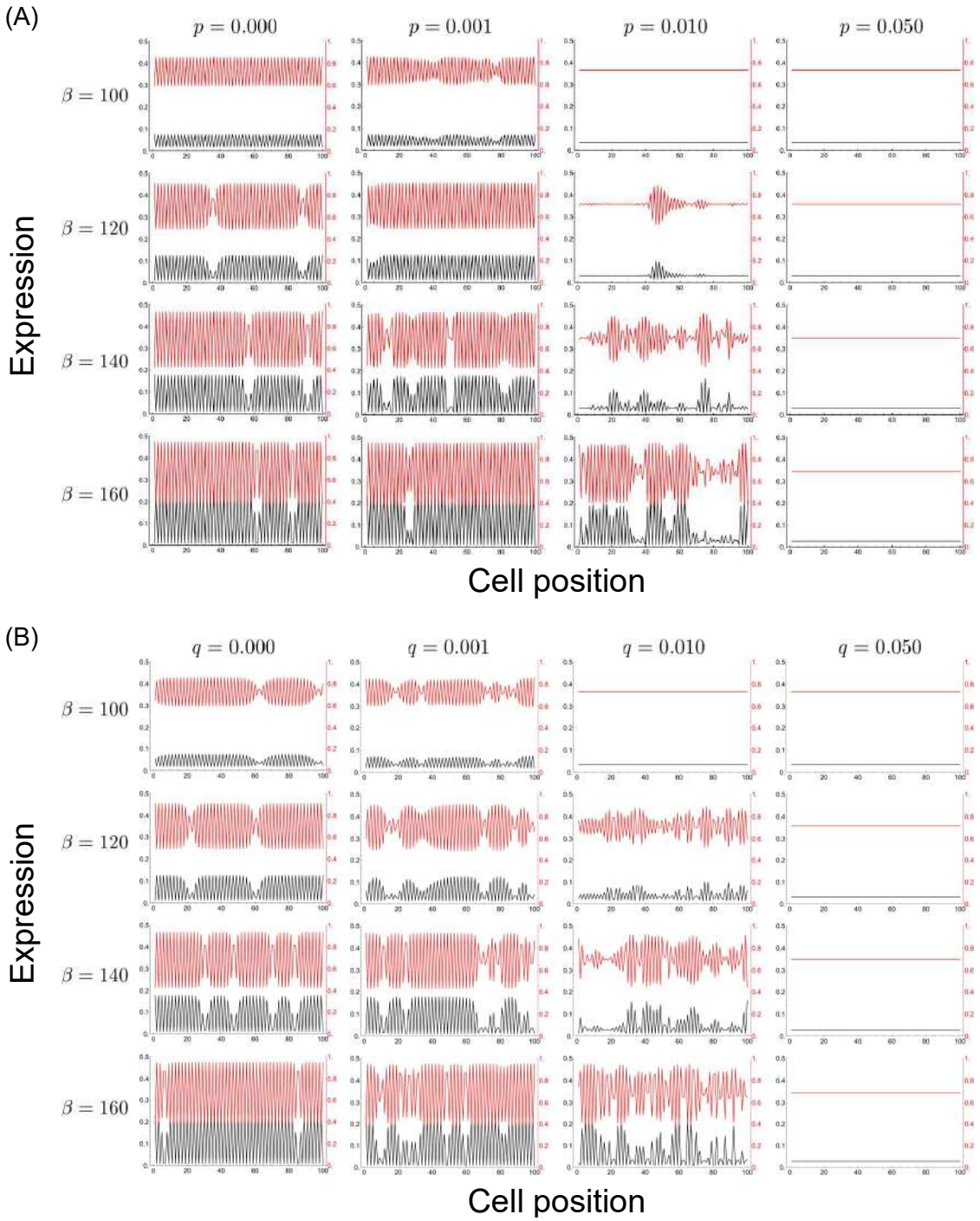

Supplementary Figure 2. Examples of the expression pattern for several values of β at $t = 10000$ in (A) cell mixing model and (B) cell proliferation model.

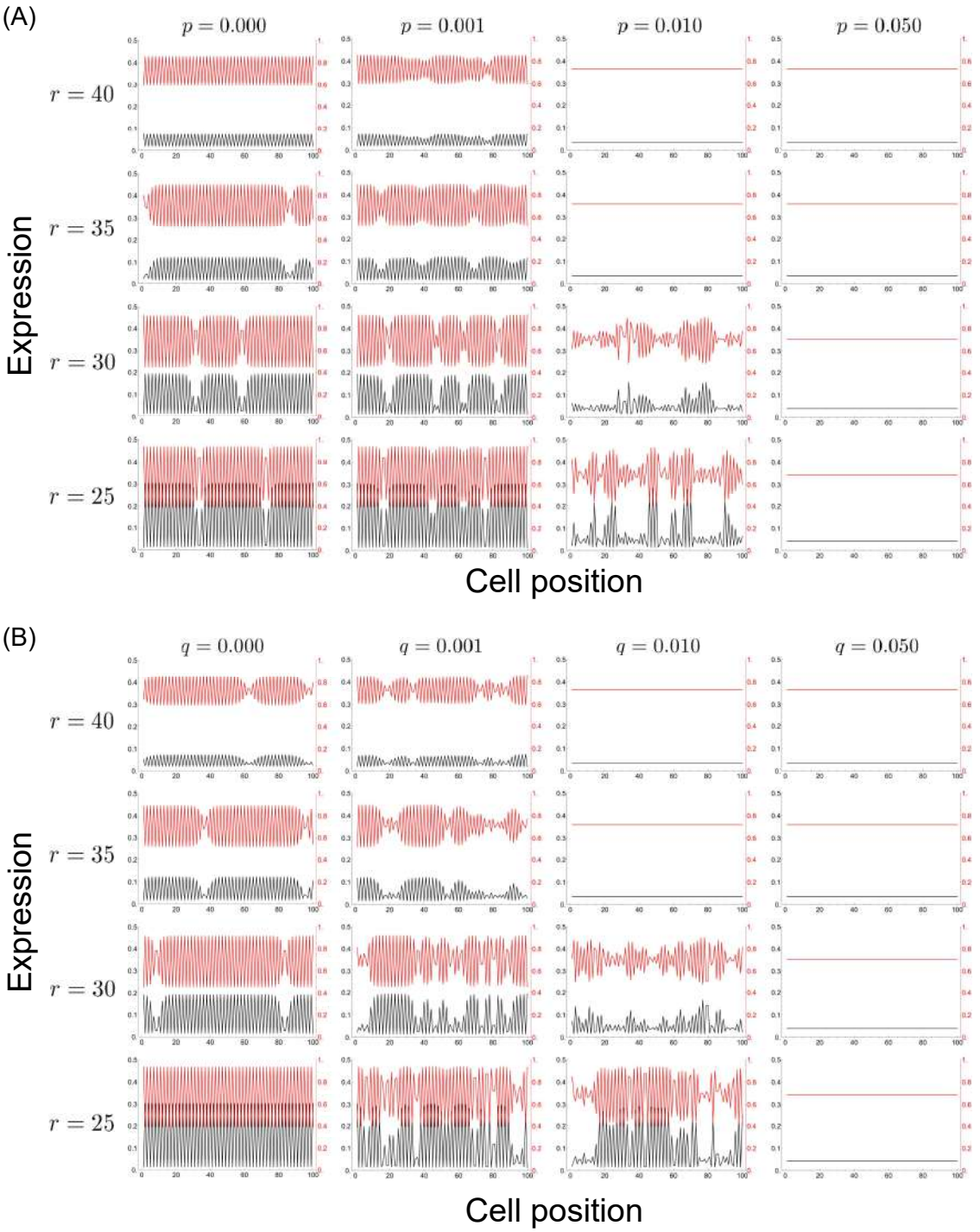

Supplementary Figure 3. Examples of the expression pattern for several values of r at $t = 10000$ in (A) cell mixing model and (B) cell proliferation model.

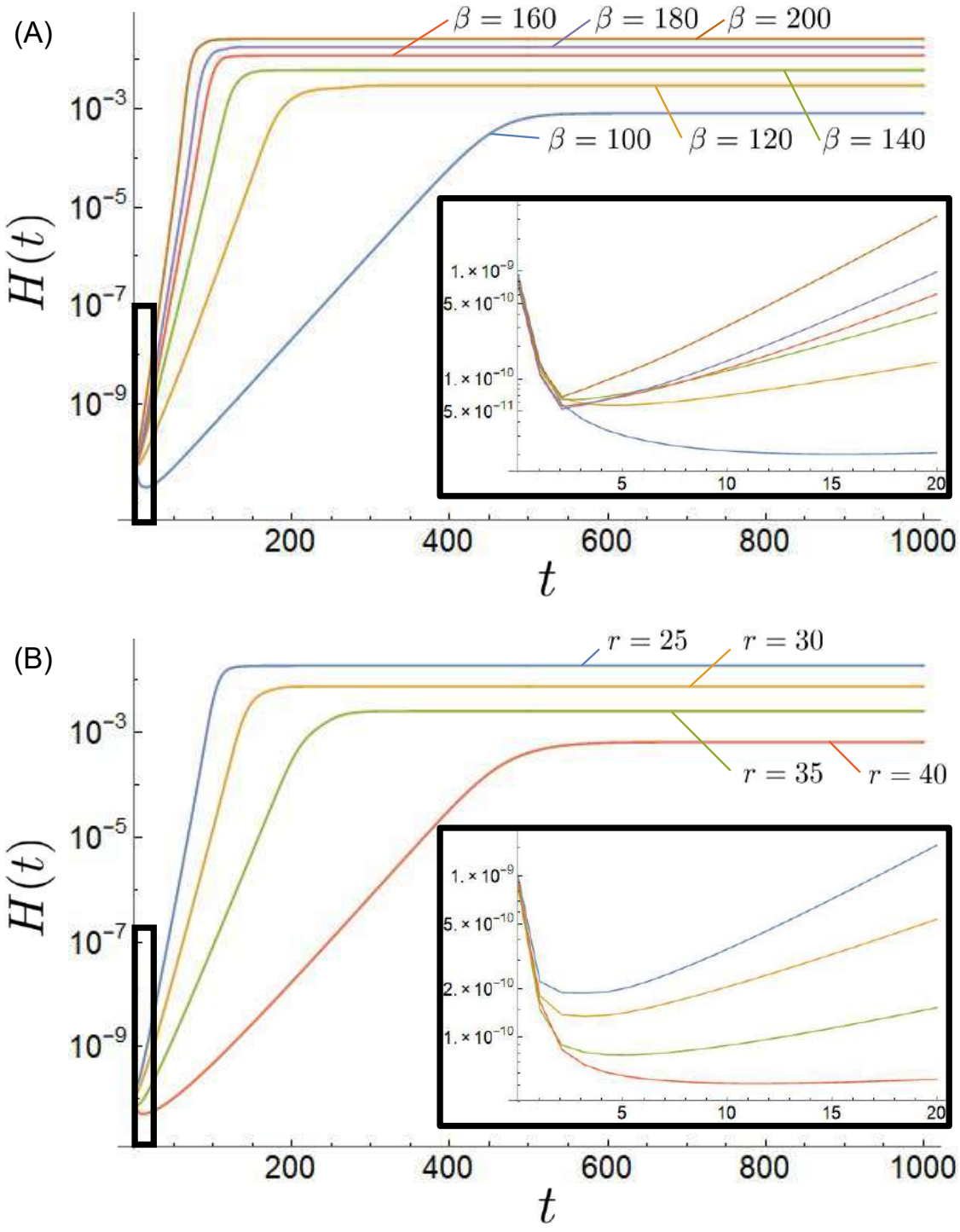

Supplementary Figure 4. Time evolution of $H(t)$ without the cell rearrangement events. (A) The time evolution of $H(t)$ for different values of β. (B) The time evolution of $H(t)$ for different values of r. The inset is the magnification of the domain $t \in [0, 20]$. $H(t)$ initially decreases and the time at which it starts to increase depends on the values of β and r.

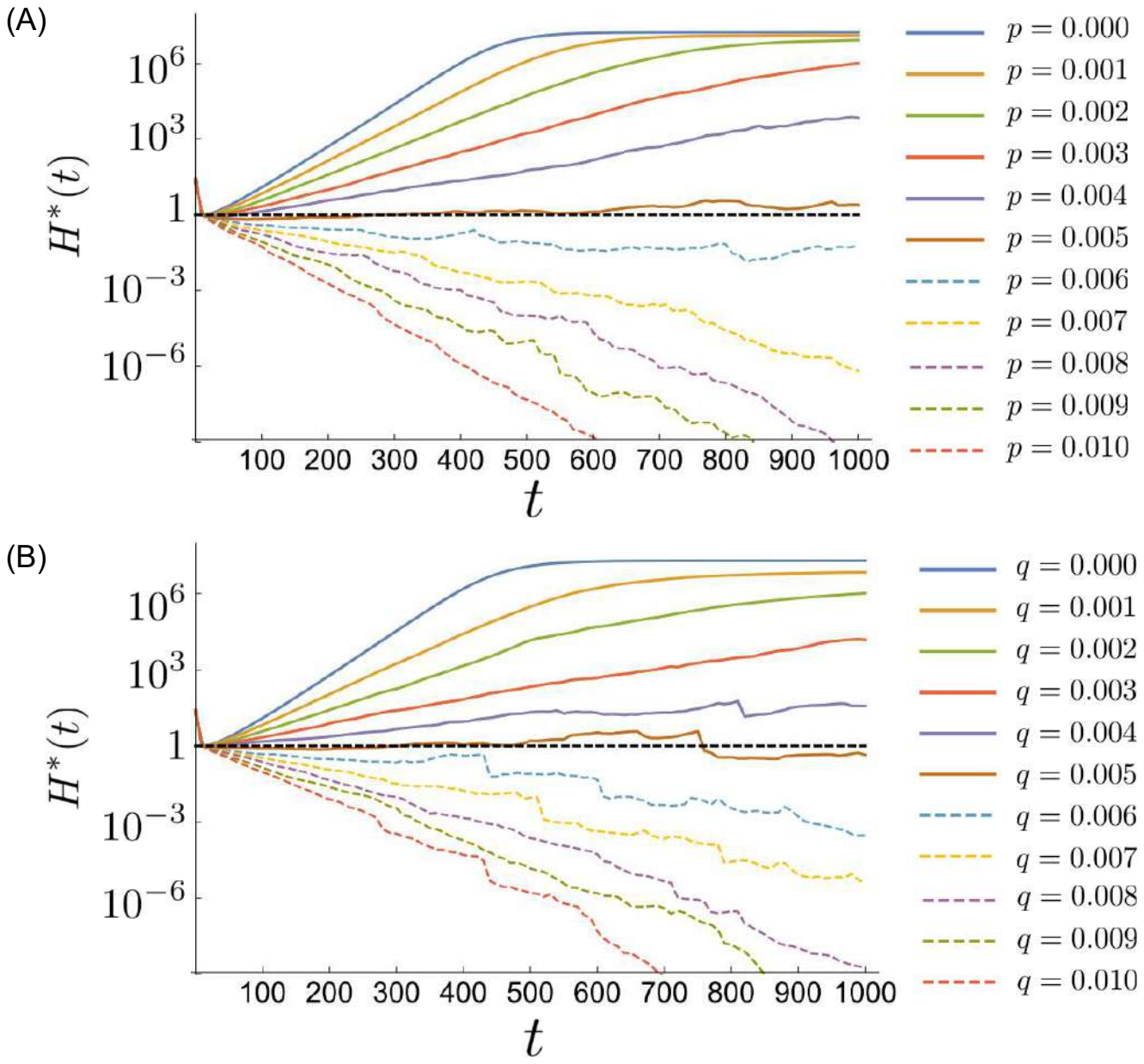

Supplementary Figure 5. Plots of the normalized heterogeneity $H^*(t)$ against time t. The heterogeneity $H^*(t)$ shown in this figure was obtained by averaging the value of $H(t)$ of 400 different simulations, and normalized by H_0 for each p and q. (A) Time evolution of $H^*(t)$ in the cell mixing model. $H^*(t)$ increases for $p \leq 0.0045$ and decreases for $p \geq 0.006$. (B) Time evolution of $H^*(t)$ in the cell proliferation model. $H^*(t)$ increases for $q \leq 0.004$ and decreases for $q \geq 0.006$. Other parameter values and initial conditions are as in Fig. 2.

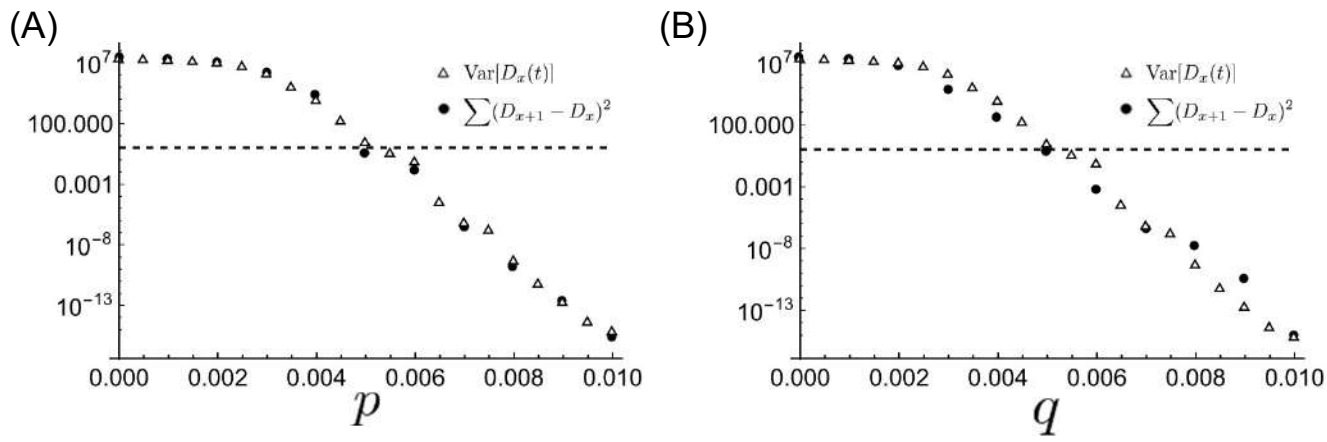

Supplementary Figure 6. Comparison of the different definitions of heterogeneity. Triangles represent the variance of D_x and black dots represent the average of $(D_{x+1} - D_x)^2$ in the cell mixing model (A) and the cell proliferation model (B). The heterogeneity function $H^*(t)$ shown in this figure was obtained by averaging the $H(t)$ value of 400 different simulations, and normalized by H_0. The triangles are the values shown in Fig. 3 for $t = 1000$. The conditions and parameter values are as in Fig. 2.

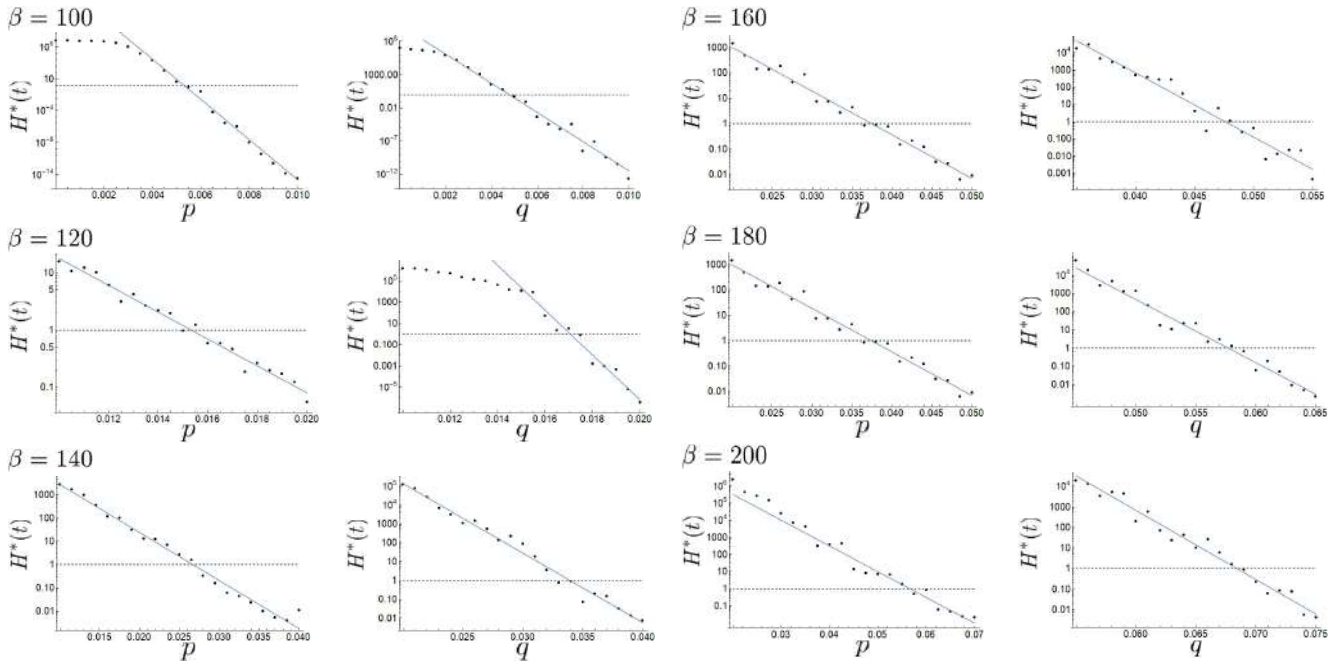

Supplementary Figure 7. The plot of $H^*(1000)$ for different values of β, corresponding to Fig. 3. The black dots are the averaged value of $H^*(1000)$. The blue line is the fitted line for the data in the range $10^{-4} < H^*(1000) < 10^4$. We numerically estimated the values of p^* and q^* as the intersection of the fitted line and $H^*(1000) = 1$.

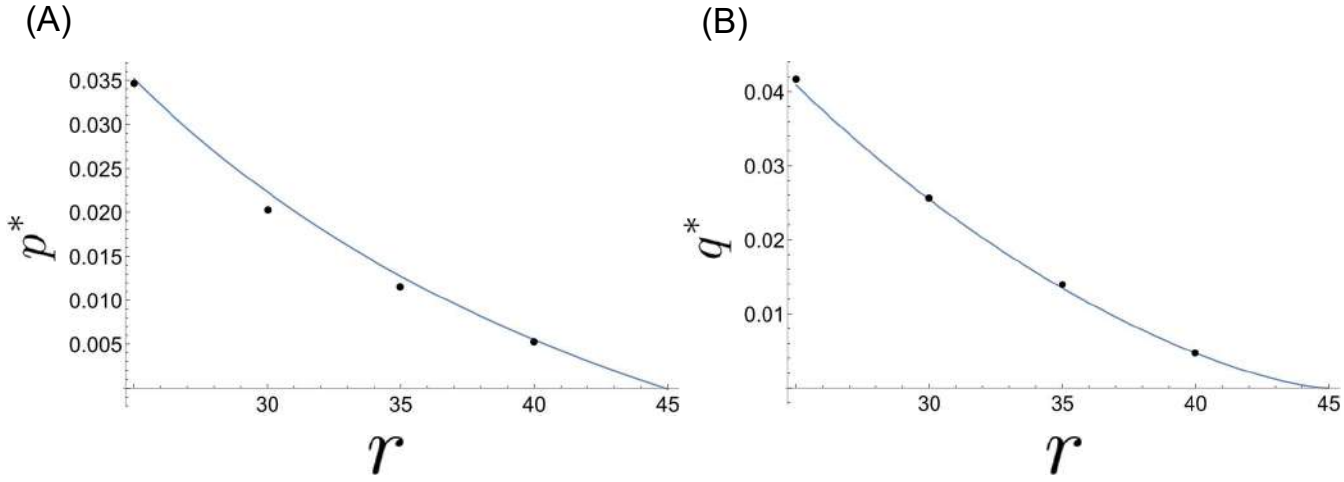

Supplementary Figure 8. The balanced frequencies p^* (A) and q^* (B) are plotted against the parameter r in the Collier model (1), corresponding to Fig. 4. The blue solid line represents the values of p such that the maximum eigenvalue of Y_p in (23) is 0, and the black dots represent the values of p^* and q^* that were estimated as in Figs. 4(C) and 4(F).

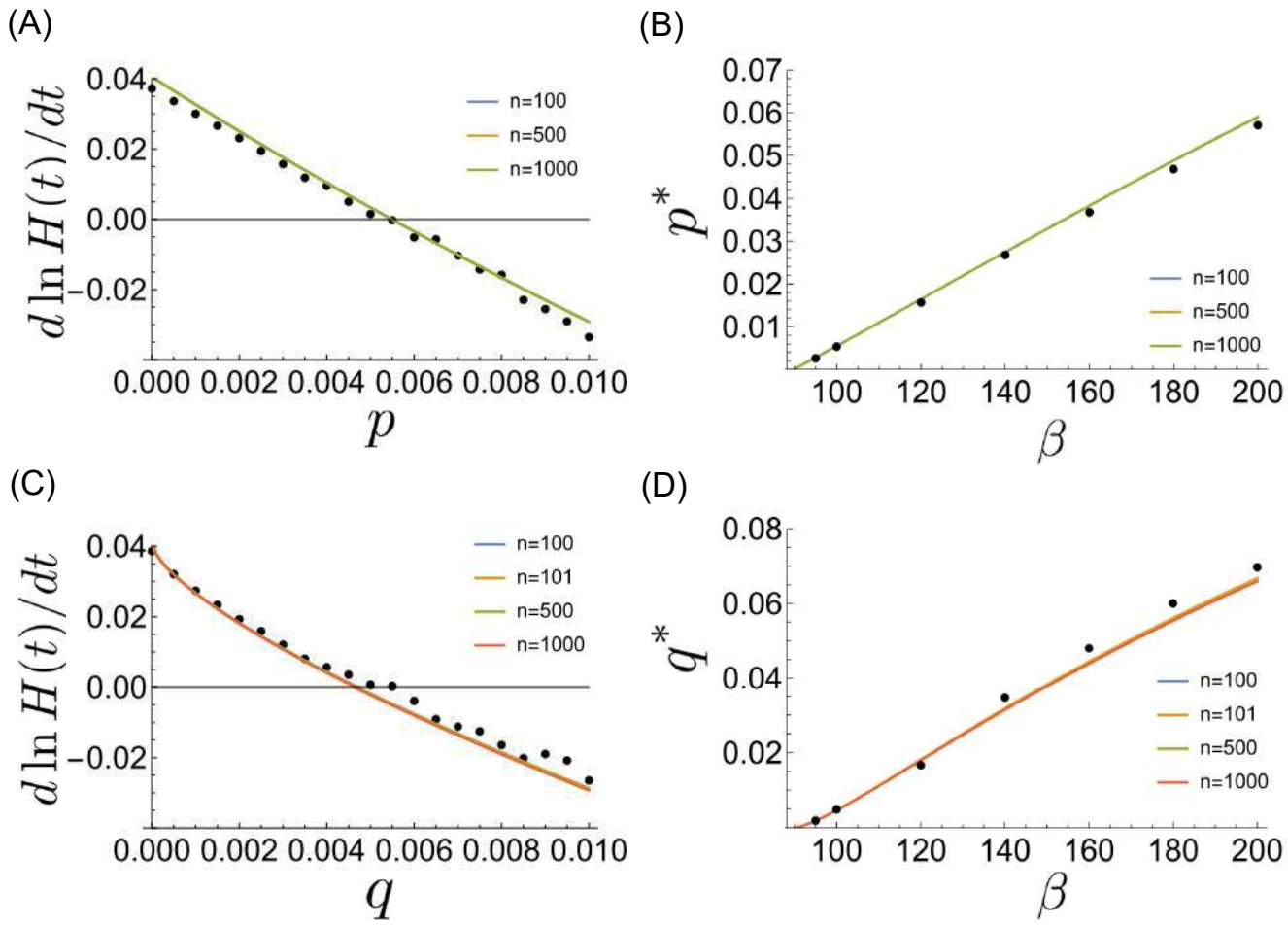

Supplementary Figure 9. Analytical results for different cell numbers. (A) Solid lines represent the maximum eigenvalue y derived from the matrix Y_p in (23) at different cell numbers ($n = 100, 500, 1000$) and the black dots are the growth rate $d \ln H(t)/dt$ estimated from Fig. S1(A), corresponding to Fig. 4(A). (B) Solid lines represent p^* derived from (23) at different cell numbers ($n = 100, 500, 1000$), and the black dots represent the p^* values that were estimated from Fig. 3(A), corresponding to Fig. 4(C). (C) Solid lines represent the maximum eigenvalue derived from the matrix J_q (39) at different cell numbers ($n = 100, 101, 500$ and 1000), and the black dots are the growth rate $d \ln H(t)/dt$ estimated from Fig. S1(B), corresponding to Fig. 4(D). (D) Solid lines represent the values of q^* derived from the matrix J_q in (39) at different cell numbers ($n = 100, 101, 500, 1000$), and the black dots represent the q^* values that were estimated from Fig. 3(B), corresponding to Fig. 4(F).

.

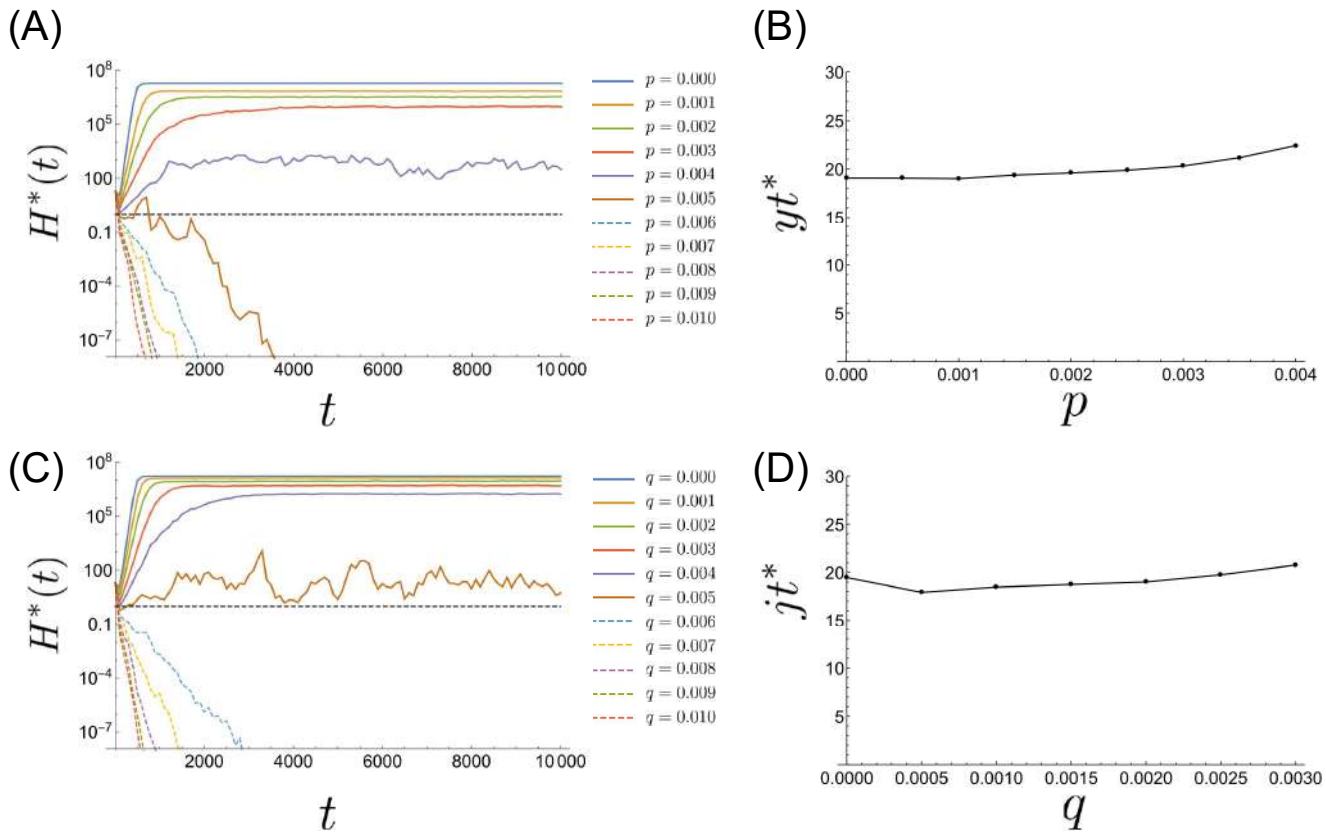

Supplementary Figure 10. The time evolution of $H^*(t)$ up to $t = 10000$. (A) $H^*(t)$ in the cell mixing model. $H^*(t)$ converged to similar order values for different p values less than 0.004, but the time to reach a steady state value increases as p increases. The black dashed line represents $H^*(t) = 1$. (B) Product of the maximum eigenvalue y in (23) and the characteristic time t^*. The values of the product are similar to each other to within an error margin of 8.2 %. (C) $H^*(t)$ in the cell proliferation model. $H^*(t)$ converged to similar order values for different p over 0.003, and the time to reach a steady state value increases as q increases. The black dashed line represents $H^*(t) = 1$. (D) Product of the maximum eigenvalue j in (39) and the characteristic time t^*. The values of the product are similar to each other to within an error margin of 7.3 %. We defined the characteristic time t^* as the time for $H^*(t)$ to reach $H^*(10000)/e$.

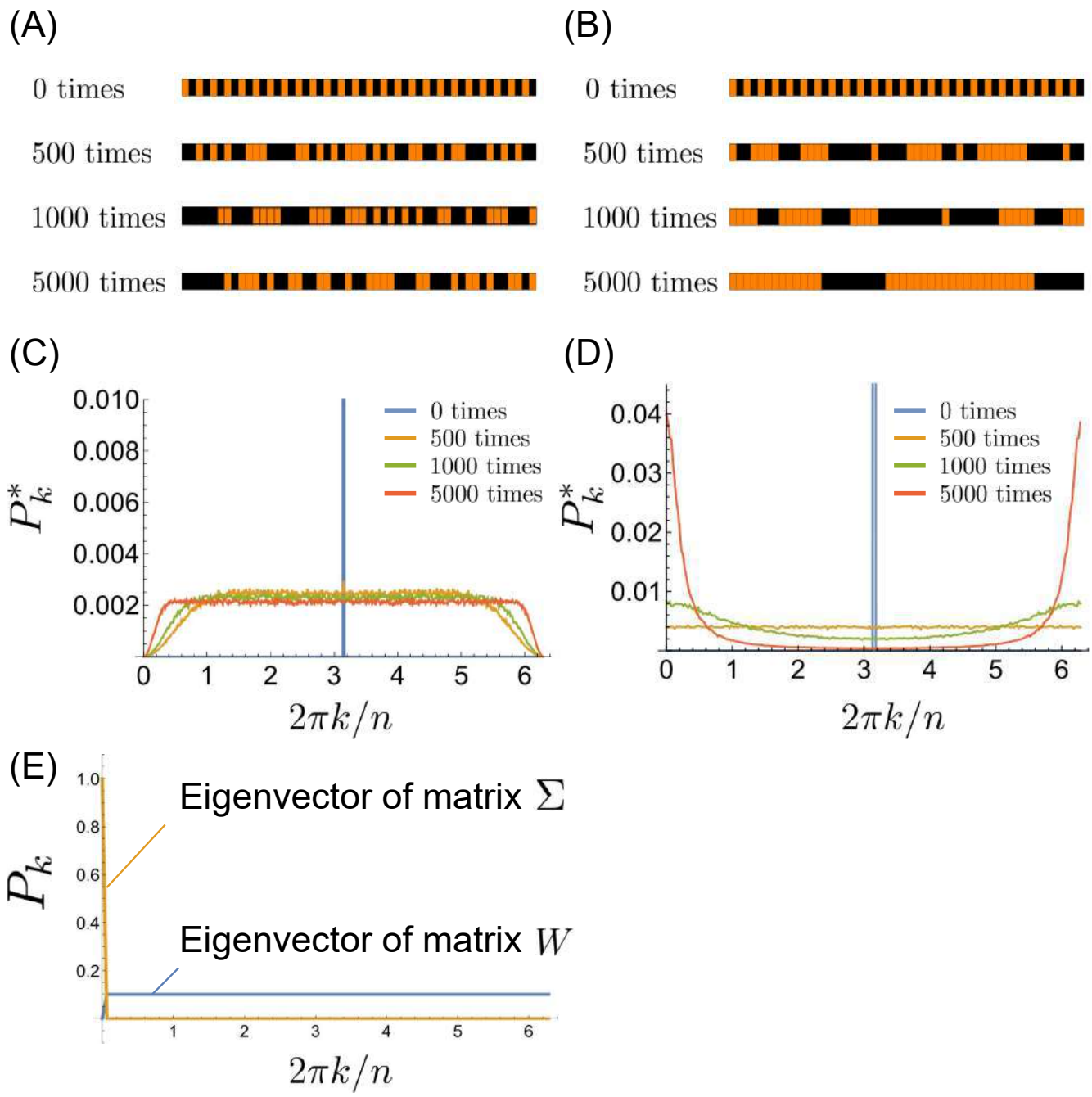

Supplementary Figure 11. Effect of cell mixing and proliferation on the existing pattern. (A,B) Example of pattern evolution from the theoretical models that include only cell mixing (A) or only proliferation (B) and excluding Delta-Notch interaction. For visibility reasons, the first 50 consecutive cells were extracted and shown. We set the salt and pepper pattern as the initial pattern. Orange cells have the expression value 1 and black cells have the expression value 0. 50 consecutive cells are extracted from the whole length and shown. (C,D) Distribution of the power spectrum of the pattern shown in (A) and (B), respectively. The average of 500 trials were plotted.

Supplementary Figure 11. (continued) (E) The eigenvectors corresponding to the maximum eigenvalue of the matrix W in (22) and the matrix Σ in (37) and (38). The eigenvector of W is uniformly distributed in $[0, 2\pi)$ and the eigenvector of Σ takes a non-zero value only at $k = 0$.

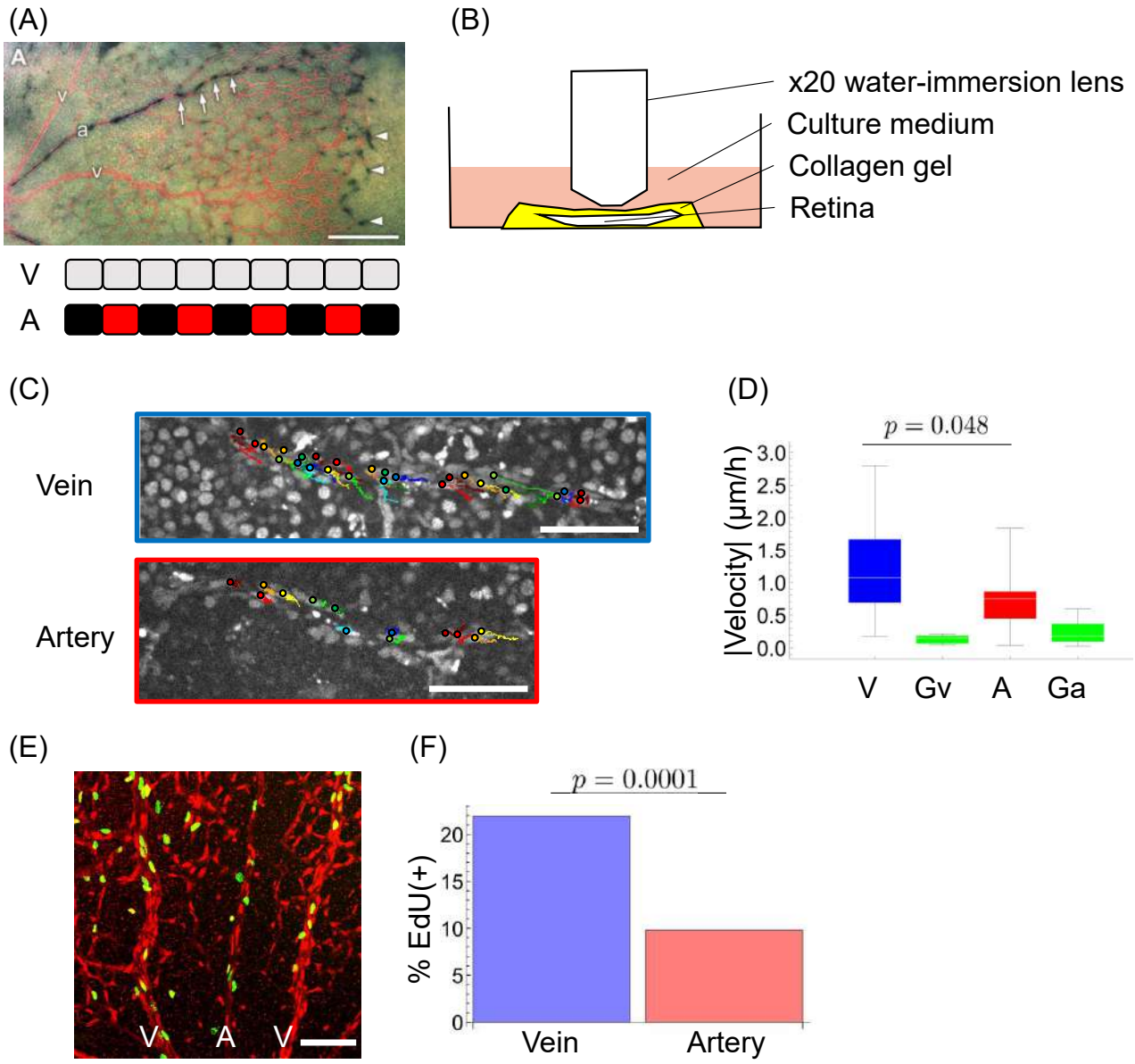

Supplementary Figure 12. Experimental assay of cell movement and proliferation. (A) Dll4 expression for endothelial cells in the retinal vasculature. Adapted from Claxton *et al.* [13]. Endothelial cells are visualized by immunostaining for type IV collagen (red), and Dll4 mRNA is visualized by in situ hybridization (black). Scale bar = 200 μm. Dll4 expressing cells are rarely observed in veins, while they are alternately aligned in arteries [8, 13, 14]. (B) Scheme of the experimental setup for retinal organ culture. Disected retina was placed on the bottom of the dish, and embedded in collagen gel. (C) Tracking of the nuclei of endothelial cells in vein (upper panel) and artery (lower panel). The lines indicate the paths of individual endothelial cells for 20 min and the dots indicate the position of the cells at $t = 720$ min. Scale bar = 100 μm.

Supplementary Figure 12. (continued) (D) Box chart for the averaged velocities of the endothelial cells in (B). Endothelial cells move at an average speed of 1.20 µm/h in veins ($n = 24$, denoted by "V"), 0.74 µm/h in arteries ($n = 13$, denoted by "A") and ganglion cells move at 0.16 µm/h near veins ($n = 10$, denoted by "Gv") and 0.23 µm/h near arteries ($n = 10$, denoted by "Ga"). Velocity here, means relative velocity, and calculated by subtracting the migration vector of the center of gravity of each cell group. P-value between endothelial cells in the veins and in the arteries is 0.048 (Student t-test). (E) Confocal microscopy images of endothelial cells stained for ERG1 (Red) and EdU (Green) in the retinal vasculature. "V" indicates veins, and "A" indicates arteries. The vessel type was distinguished by anatomical features such as the avascular zone and the thickness of the vessel. Scale bar = 100 µm. (F) Bar chart of the fraction of the EdU(+) endothelial cells. 21.9% (93/424) of venous endothelial cells and 9.8% (20/204) of arterial endothelial cells are positive for EdU. P-value is 0.0001 (Fisher's exact test).

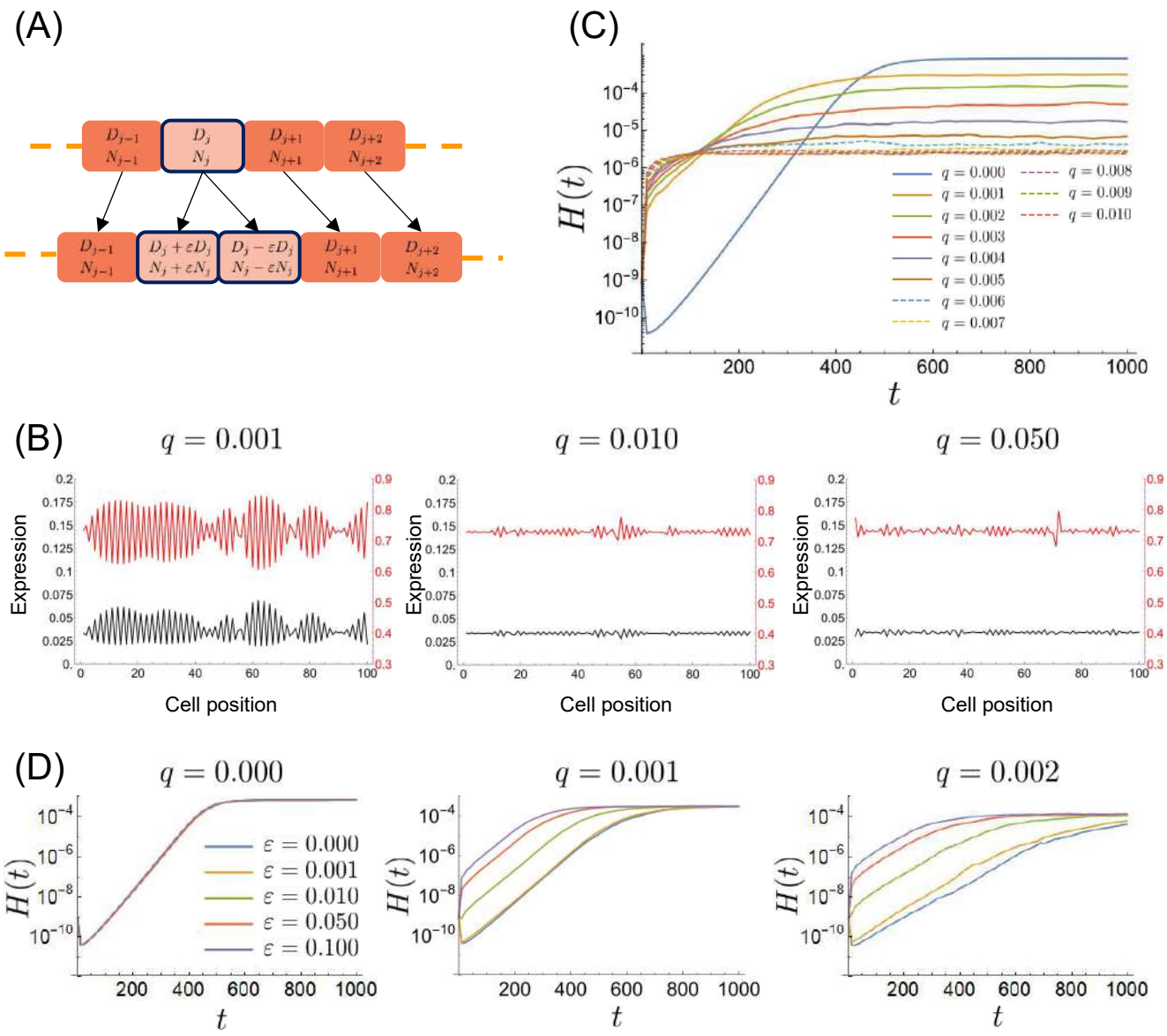

Supplementary Figure 13. Cell proliferation model with asymmetric inheritance rules. (A) Schematic of the asymmetric inheritance rules. The Delta and Notch activities of the daughter cells are $D_x \pm \bar{\varepsilon} D_x$ and $N_x \pm \bar{\varepsilon} N_x$, respectively. The value of $\bar{\varepsilon}$ is a random variable following the uniform distribution $U(-\varepsilon, \varepsilon)$. (B) Example of the expression pattern of the cell proliferation model with asymmetric inheritance rules. The red line represents Notch expression and the black line represents Delta expression. As q increases, the amplitude of the pattern gets smaller, but the amplitude does not converge to 0. (C) Time evolution for $H(t)$ with different values of q. We set $\varepsilon = 0.1$, and the other parameters are the same as in Fig. 2. (D) Time evolution of $H(t)$ with different values of ε and q.

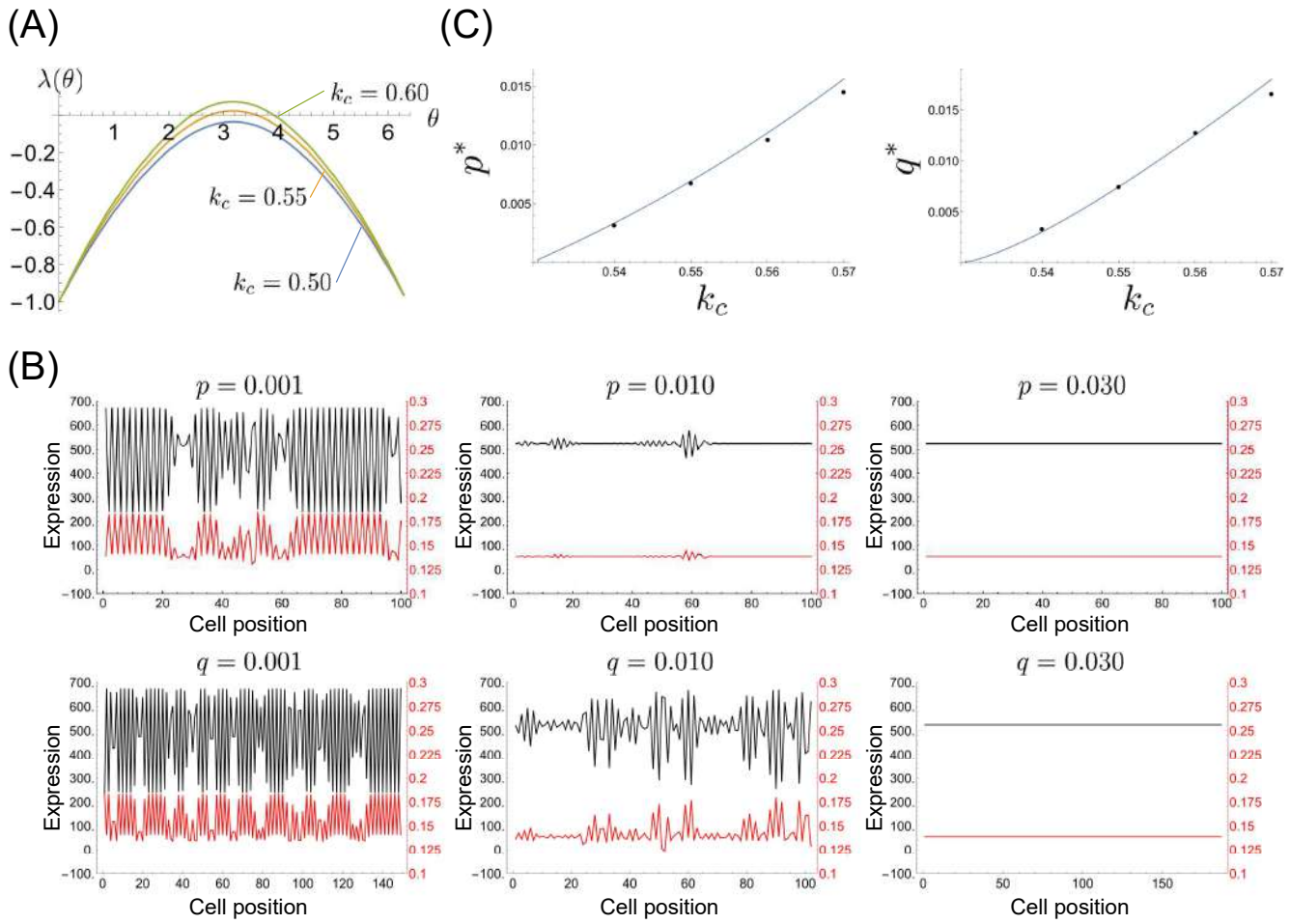

Supplementary Figure 14. Numerical and analytical results for the Sprinzak model (S47). (A) The dispersion-relation of the Sprinzak model for different values of k_c. (B) Example of the expression pattern of the cell mixing model (upper panels) and the cell proliferation model (lower panels). Similar to the Collier model, as the frequencies of the cell rearrangement events p and q increase, the amplitude of the pattern decreases and the homogeneous steady state becomes stable. (C) The balanced frequencies p^* (left panel) and q^* (right panel) against k_c. The blue line represents p^* and q^* obtained by the same analysis we used for the Collier model, and the black dots represent the numerical estimation of p^* and q^*. Conditions for numerical simulations; Initial cell number $n = 100$, time step $\Delta t = 0.001$, duration $t = 1000$ (iteration 1000000), and $(k_{rs}, \beta_n, \beta_d, \beta_r, m) = (300000, 200, 1000, 3000, 3)$. Initial conditions are $N_x(0) = N^0(1+\kappa)$, $D_x(0) = D^0(1+\kappa)$ and $R_x(0) = R^0(1+\kappa)$. Here N^0, D^0 and R^0 are the spatially homogeneous steady state (Supplementary text C [28]), and κ is a random variable from the uniform distribution in $[-0.01, 0.01]$.